A Lattice Relaxation Algorithm for Three-Dimensional Poisson-Nernst-Planck Theory with Application to Ion Transport through the Gramicidin A Channel

Maria G. Kurnikova,* Rob D. Coalson,* Peter Graf,# and Abraham Nitzan#
*Department of Chemistry, University of Pittsburgh, Pittsburgh, Pennsylvania 15260, USA and #Department of Chemistry, Tel Aviv University, Tel Aviv, 69978 Israel

ABSTRACT A lattice relaxation algorithm is developed to solve the Poisson-Nernst-Planck (PNP) equations for ion transport through arbitrary three-dimensional volumes. Calculations of systems characterized by simple parallel plate and cylindrical pore geometries are presented in order to calibrate the accuracy of the method. A study of ion transport through gramicidin A dimer is carried out within this PNP framework. Good agreement with experimental measurements is obtained. Strengths and weaknesses of the PNP approach are discussed.

INTRODUCTION

The mechanism and properties of ion transport through channel proteins embedded in lipid bilayers (e.g., cell walls) is a subject of wide current interest (Hille, 1992; Cooper et al., 1985; Fishman, 1985; Eisenberg, 1996, 1998). These structures provide gates for ions like Na^+, Cl^-, K^+, and Ca^{2+} to enter or leave the cell. By regulating passage through these gates, cells can maintain desired internal ion concentrations (which are often quite different from their concentration in the surrounding bulk solution) (Aidley and Stanfield, 1996). Important functions such as energy storage and signal transduction are also mediated via ion flow through biological pores.

Theoretical treatments of ion transport through channel proteins may be broadly classified as kinetic models, electrodiffusion models, and stochastic models (Cooper et al., 1985). One expects that with progress in computing power and techniques, molecular dynamics (MD) methods (Roux and Karplus, 1993; Elber et al., 1995) will also become increasingly useful. Here we focus on the electrodiffusion framework, in which the mobile ions are represented as a continuous charge density and the dynamics is described by the Poisson-Nernst-Planck (PNP) theory (see, for example, Eisenberg (1996) and references therein). PNP theory combines Nernst-Planck theory of electrodiffusion with the recognition that the electric field established in the channel interior depends on the concentration profile of the mobile ions in it. The latter feature results in the need to solve the Poisson equation of electrostatics including contributions to the electrical charge density arising from the mobile ion concentration in the channel. Ultimately, PNP theory requires self-consistent solution of the Poisson equation and drift-diffusion equations for all the ionic species moving through the channel.

The PNP theory of electrodiffusion has for a long time been applied to liquid junctions and membrane electrochemistry (see, e.g., Newman (1991)). Numerical solutions of these nonlinear partial differential equations for ionic transport at liquid junctions demonstrated the limits of linearized approximations used in analytical solutions, and the relevance of this observation to ion transport through the membrane channel was suggested (Riveros et al., 1989). Due to their relative complexity, actual applications within the latter context have been restricted to simplified geometries and involved simplifying assumptions (Levitt, 1991a, b; Barcilon et al., 1992; Chen et al., 1992; Syganow and von Kitzing, 1995; Chernyak, 1995; Woolley et al., 1997). A fully self-consistent solution of the coupled PNP equations for three-dimensional (3D) systems was first targeted for a cylindrical channel model in Barcilon et al. (1992) and Chen et al. (1992). The resulting set of equations, in leading order and certain limits which reduce the 3D equations to a 1D representation, has been applied to various channel systems (Barcilon et al., 1992; Chen et al., 1992; Chen and Eisenberg, 1993a, b; Chen et al., 1997a, b). Such a reduction, however, is not possible a priori in the general case of arbitrary channel geometry and complicated nonsymmetric assembly of partial electric charges embedded in the protein. Clearly, a realistic description of the ion channel system must in general be three-dimensional. It requires knowledge of the 3D structure of the channel protein in the lipid membrane. Presently, several 3D channel structures are known to high precision (Venkatchalam and Urri, 1983; Unwin, 1995; Cowan et al., 1992; Weiss and Schulz, 1992; Kreusch and Schulz, 1992; Song et al., 1996; Doyle et al., 1998). Given reliable information about the channel structure, one then needs the mathematical methodology and computational resources to solve the PNP equations numerically. We note that the special case of the PNP problem corresponding to no ion flow, i.e., when the mobile ions are in thermal equilibrium with their surroundings, has been

Received for publication 16 June 1998 and in final form 14 September 1998.

Address reprint requests to Dr. Rob D. Coalson, Dept. of Chemistry, University of Pittsburgh, Pittsburgh, PA 15260. Tel.: 412-624-8261; Fax: 412-624-8611; E-mail: coalson@vms.cis.pitt.edu.

0006-3495/99/02/642/15 $2.00

extensively scrutinized via 3D modeling. In this case, the PNP equations reduce to the Poisson-Boltzmann equation, for which flexible, efficient, and reliable numerical solution procedures exist (Nicholls et al., 1990; Luty et al., 1992; Coalson and Duncan, 1992; Walsh and Coalson, 1994; Ben-Tal and Coalson, 1994).

The purpose of the present paper is to apply similar numerical techniques to solve the 3D steady-state PNP equations under rather general conditions: arbitrary macroion geometries, charge distributions embedded in the macroions, dielectric constant profiles, etc. The application to calculation of the current through the gramicidin A channel demonstrates that the continuum theory approach can give valuable insight into the understanding of ion-channel interactions.

Representing the mobile ions as a charge density and the protein and water environment as dielectric continua obviously ignores potentially important molecular characteristics of the system. For example, the nature of the ion solvation changes upon entering a narrow channel and this change is not easy to include in a continuum theory. Even within the framework of PNP theory, one sometimes must choose values for parameters which are not available from experimental studies. We have utilized the simplest physically justifiable parameters in such instances. For example, we use constant ionic concentrations in the intracelluar and the outer reservoirs, even very close to the membrane and the entrance of the channel. One could argue that the ionic distribution should not be uniform near the channel entrance and exit, but it is not known at present what this distribution should be. [Note that models for this charge distribution, and the associated "access resistance," have recently been discussed within the PNP framework (Chen and Eisenberg, 1993a; Ramanan et al., 1994; Novak, 1997).] Despite the limitations outlined above, our calculation demonstrates that with careful 3D modeling of the channel based on the experimentally determined channel structure, the results obtained using PNP theory compare well to those obtained in experimental studies.

The outline of the paper is as follows. In Theory, essential elements of the PNP theory are briefly reviewed. The details of the numerical solution of the 3D PNP equations for an arbitrarily shaped and charged channel are described in Computational Methods. Calibration of the Accuracy of the 3D code presents calculations on prototypical parallel plate and cylinder systems designed to calibrate the accuracy of our 3D algorithm. Then, in the next section, 3D PNP theory is applied to calculation of the ionic current through the gramicidin A channel. Finally, discussion and conclusions are presented.

THEORY

The steady-state PNP procedure combines steady-state solutions of the Smoluchowski equation with solutions of the Poisson equation, performed self-consistently. It is perhaps most easily explained by initially considering motion of a Brownian particle in a prescribed external potential $V(\vec{R})$ ($\vec{R}$ being the particle's position) under conditions of high friction, where the Smoluchowski equation applies (Chandrasekhar, 1943).

Steady-state solutions of the Smoluchowski equation

The Smoluchowski equation (SE) details the time-evolution of the probability distribution of the Brownian particle, or, equivalently, the concentration dependence $c(\vec{R}, t)$ of an ensemble of these particles. It has the form of a continuity equation:

$$\frac{\partial c(\vec{R}, t)}{\partial t} = -\vec{\nabla} \cdot \vec{j}(\vec{R}, t) \tag{1}$$

where the particle flux is given by:

$$\vec{j}(\vec{R}, t) = -D[\vec{\nabla} c(\vec{R}, t) + \beta \vec{\nabla} V(\vec{R}) c(\vec{R}, t)] \tag{2}$$

with D the diffusion constant and $\beta = 1/kT$ (k is Boltzmann's constant and T the absolute temperature). The two terms contributing to the flux have clear physical meanings. The first is due to diffusional processes, as quantified by Fick's first law. The second contribution is due to the drift velocity $-\vec{\nabla} V(\vec{R})/\eta$ induced by the systematic external force $-\vec{\nabla} V(\vec{R})$ and friction quantified by the friction constant η. (The Stokes-Einstein relation $D = kT/\eta$ is then invoked to obtain the second term on the r.h.s. of Eq. 2.)

We are interested in steady-state solutions, i.e., $\partial c(\vec{R}, t)/\partial t = 0$ everywhere. The flux $\vec{j}$ then also becomes time-independent. Any steady-state solution of the SE satisfies the equation $0 = \vec{\nabla} \cdot \vec{j}$, or equivalently:

$$0 = \vec{\nabla} \cdot [\vec{\nabla} c(\vec{R}) + \beta \vec{\nabla} V(\vec{R}) c(\vec{R})] \tag{3}$$

Given $c(\vec{R})$ on the boundary surface, this equation has a unique interior solution. Once the solution has been computed it is easy to determine the value of the flux vector to which it corresponds at any point in space (cf. Eq. 2).

Many ionic species and electrostatic interactions

In the problem of ion diffusion through channels two additional complications arise. First, the potential felt by each ion includes, in addition to effects of short-range forces (hard or soft core repulsion from atoms forming the channel wall), long-range electrostatic interactions with other charged species in the system. Second, there are in general several ionic species. In the standard, mean field approximation, direct correlation between the motion of ions in the channel is neglected. Hence we write the total potential energy experienced by the ith ion species as:

$$V_i(\vec{R}) = U(\vec{R}) + z_i e \phi(\vec{R}) \tag{4}$$

Here $U(\vec{R})$ is the potential due to nonelectrostatic interactions, which for simplicity is assumed identical for all ion species. $\phi(\vec{R})$ is the electrostatic potential, z_i is the ion's valence, and e is the magnitude of the charge of the electron. The electrostatic potential ϕ depends on the distribution of charges in the system, as well as the dielectric constant profile and the assumed boundary values (due, for example, to an external voltage applied across the system). ϕ is determined by solving the Poisson equation self-consistently with steady-state SE's for each ionic species (below).

Thus, the PNP procedure requires us to solve the Poisson equation taking into account all charges present in the system. These are of two types, charges which are embedded in the membrane protein, and charges carried by the mobile ions. Since the density of mobile ions depends on the solution of the SE, and the solution of the SE depends on the electric potential, the following set of equations must be solved:

$$0 = \vec{\nabla} \cdot [\vec{\nabla} c_i(\vec{R}) + \beta \vec{\nabla} V_i(\vec{R}) c_i(\vec{R})]; \quad i = 1, \ldots, N \qquad (5)$$

The Poisson equation must be solved self-consistently with these:

$$\vec{\nabla} \cdot (\epsilon(\vec{R}) \vec{\nabla} \phi(\vec{R})) = -4\pi \left[\rho_f(\vec{R}) + \sum_{i=1}^{N} z_i e c_i(\vec{R}) \right]; \qquad (6)$$

here i labels the ionic species, ϵ is the dielectric constant profile, and ρ_f is the density of fixed charges embedded in the macroions found in the system (e.g., the channel protein). The steady-state SE's appearing in Eq. 5 are often referred to as "drift-diffusion" equations [for example, in the semiconductor device design literature (Selberherr, 1984)] and as "Nernst-Planck" (NP) equations [for example, in the biophysics community (Barcilon et al., 1992)]. Below we use these designations interchangeably.

COMPUTATIONAL METHODS

While the form of the PNP Eqs. 5 and 6 is well known, explicit solution in 3D has only been attempted in a few cases, all of which to our knowledge have arisen in the context of semiconductor device design (Selberherr, 1984). In this work we develop a simple, reliable, and efficient lattice relaxation scheme which parallels widely used methods for solving the Poisson and Poisson-Boltzmann equations in biophysical (Nicholls et al., 1990; Luty et al., 1992) and colloid science (Coalson and Duncan, 1992; Walsh and Coalson, 1994; Ben-Tal and Coalson, 1994) applications. Two algorithms for solving the NP Eq. 5 are described in Appendices 1 and 2. In Appendix 1 we use the Slotboom transformation (Slotboom, 1969) in order to transform the NP equation to a Laplace equation (i.e., Poisson equation with no source charge) with a peculiar effective dielectric constant profile. Using the resulting Laplace equation, solution of the coupled Eqs. 5 and 6 can be obtained utilizing standard 3D lattice Poisson equation solvers (Nicholls et al., 1990; Luty et al., 1992; Coalson and Duncan, 1992; Walsh and Coalson, 1994; Ben-Tal and Coalson, 1994). We also provide, in Appendix 2, a simple, explicit Successive Over-Relaxation (SOR) (Press et al., 1992; Coalson and Beck, 1998) scheme for solving the NP equation directly, including easy and general implementation of zero-flux boundary conditions, which arise naturally in the applications of interest here. Both methods have proven effective in test calculations.

In addition to a generic computer code for solving Eqs. 5 and 6, applications to biophysical systems require a method for discretizing 3D biological structures (e.g., the channel protein and cell membrane) onto a cubic lattice. Fortunately, the same issue arises in studying electrostatic and equilibrium electrolyte properties of biophysical systems via the Poisson and Poisson-Boltzmann equations, respectively. Thus we have utilized Delphi (Nicholls et al., 1990), a well-known Poisson/Poisson-Boltzmann equation solver, which allows mapping of the protein onto a 3D grid. The Delphi source code was modified to include a procedure for wrapping a membrane around the channel protein and mapping this membrane onto the 3D grid as well. The overall system was partitioned into two regions. The first region is characterized by a low dielectric constant ϵ_m and represents the protein and the membrane in which it is embedded. The second region, representing the solvent reservoirs and the permeable channel itself, is characterized by a high dielectric constant ϵ_a. In other words $\epsilon(\vec{R})$ in Eq. 6 was set to

$$\epsilon(\vec{R}) = \begin{cases} \epsilon_m, & \text{if } \vec{R} \in \{\text{protein or membrane}\} \\ \epsilon_a, & \text{otherwise} \end{cases}$$

The protein-solvent boundary is determined as the solvent-accessible van der Waals surface using the method of Connolly (1983), as implemented in Delphi. The Delphi code was further modified to include steady-state Nernst-Planck equations (cf. Appendix 2) along with the electrostatic Poisson equation solver. Other modifications included the possibility of setting different salt concentrations in the solvent on different sides of the membrane, as well as a potential difference on opposite boundaries of the box (corresponding to an applied potential created, for example, by electrodes).

The calculations were performed on uniform cubic lattices of up to $(170)^3$ grid points. The boundary condition for the flux equation is zero current through the channel wall, i.e.:

$$\vec{j}_\perp = 0|_{\vec{R}=\vec{R}_b}, \qquad (7)$$

where $\vec{R}_b$ is a channel boundary point and $\vec{j}_\perp$ is the flux component normal to the boundary. Implementation of zero-flux boundary conditions on a cubic lattice is discussed in Appendix 2.

A fixed electric potential and ion concentrations were set on the upper and lower faces of the computational box. The channel was oriented normal to these two faces (along the z-axis). On the side faces the potential was set according to

a linear variation between upper and lower values along the vertical coordinate. Inside the membrane and protein, mobile ion concentrations were set to zero. The concentrations of the positive and negative ions were equal to each other on both top and bottom faces to ensure charge neutrality in the reservoirs. Ion concentrations were allowed to change only in the interior of the channel.

For the cylinder calculations presented below, a cylindrical hole of the desired radius oriented from top to bottom of the box was made through the membrane layer (cf. Fig. 1). The dielectric constants were set to $\epsilon_m = 2$ and $\epsilon_a = 80$. The gramicidin geometry reflects its molecular structure as described below. The choice of dielectric parameters for the gramicidin channel calculations will be discussed later.

Our program was executed on a DEC α21164a-clone workstation with 512Mb of RAM. The computational time varied from 10 min/point of the current-voltage characteristic on a $100 \times 100 \times 100$ grid, to several hours/point, depending on the external salt concentrations (at the low ionic strength the computation time required increases) and epsilon values chosen (see below).

CALIBRATION OF THE ACCURACY OF THE 3D CODE

It is a challenge to calibrate the accuracy of the full 3D PNP code, which consists of coupled lattice relaxation of 3D scalar fields representing the electrical potential and the densities of all mobile ion species. Analytical solutions exist only for a few special cases (see below). Moreover, no other computer algorithms that solve the 3D PNP equations in the context of biological channel proteins or related problems were available to us. Nevertheless, we tested our 3D PNP code against several limiting case solutions.

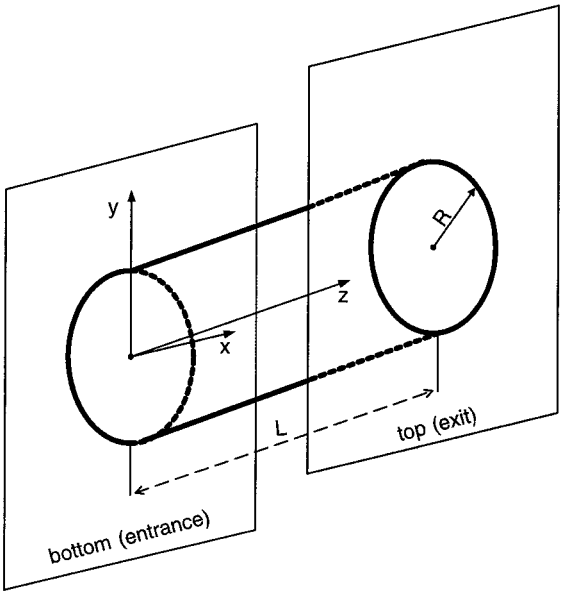

FIGURE 1 Geometry of cylindrical pore system. The coordinate system adopted in the text is shown and the radius and the length of the cylinder are indicated.

The calculations presented below assume that the salt concentrations are given at the entrance and the exit of the channel. These concentration boundary conditions are set so as to enforce charge neutrality at these positions. In the case of monovalent cations and anions, this means that the concentrations of cations and anions are the same at the entrance to the channel (label this concentration c_0) and at the exit from the channel (label this concentration c_L). [In the gramicidin channel problem discussed below, it is not known precisely whether the bulk concentration reservoirs extend right up to the entrance to the channel, as implied by the boundary conditions adopted here. Preliminary calculations on cylinder systems indicate that the current-voltage characteristic is not very sensitive to this choice. A more complete analysis of the ion flow through a cylinder within PNP theory will be presented elsewhere.]

We have focused our calibration efforts on the case that the ion channel is represented by a cylinder of length L and radius R, whose interior is a high dielectric region, $\epsilon_a = 80$, permeable to water and simple ions. The exterior of the cylinder represents the cell membrane, which is a low dielectric region with $\epsilon_m = 2$ and is impermeable to water or ions. A typical system is illustrated in Fig. 1.

For this geometry, the case of no applied voltage has a simple exact solution. Namely, the concentrations of both $\pm$ ions is given by:

$$c(z) = c_0 + (c_L - c_0)z/L \tag{8}$$

Note that the concentration is independent of the transverse directions x and y. Obviously, there is no net electric charge anywhere in the system and the voltage on the boundary of the system is zero, so the electric potential $\phi = 0$ everywhere. Equation 8 is clearly a solution of the 3D drift-diffusion equation for both $\pm$ ions when $\phi = 0$, and it satisfies the desired boundary conditions. In particular, the concentration gradient in the transverse directions (radially out from the center of the cylinder) is zero, hence (with $\phi = 0$) there is no flux through the cylinder walls, as desired. We have checked that when we solve the full 3D PNP equations by lattice relaxation for the case of zero applied potential, the solution just described emerges.

When a potential is applied on the boundaries, it polarizes the mobile charge in the middle. This generates a net charge distribution in the cylinder and makes the solution of Poisson's equation and, in turn, the solution of the drift-diffusion equations considerably more complex. At steady state the electric potential and ion concentrations are complicated functions of z and $r = \sqrt{x^2 + y^2}$, for which no analytical solution is apparent. However, we can partially test our code by imposing an electric potential $\phi(z)$ which is independent of x and y, but otherwise arbitrary. Given only two types of monovalent ions, namely, cations of concentration c^+ and anions of concentration c^-, with equal diffusion coefficients, the steady-state concentration profiles inside the

cylinder are also independent of x and y, and can be obtained by using the formula:

$$c^{\pm}(z) = \exp[\mp\bar{\phi}(z)]\{c_0\exp(\pm\bar{\phi}_0)[S(L) - S(z)] + c_L\exp(\pm\bar{\phi}_L)S(z)\}/S(L) \quad (9)$$

with $\bar{\phi} = e\phi/kT$ and

$$S(z) \equiv \int_0^z dz' \exp[\pm\bar{\phi}(z')]$$

In Fig. 2 we show the variation of positive ion density with z along the channel center when a linear potential ramp $V_0 - V_L = 200$ mV is applied, and the concentrations at the entrance and exit of the cylinder channel are $c_0 = 25$ mM and $c_L = 3$ mM, respectively, at a temperature of 25°C (i.e., $kT = 25.7$ meV). 3D solutions of the NP equations using various grid sizes are compared to the 1D result given by Eq. 9 (specialized to the case of a linear potential profile). It is clear that the 3D result approaches the 1D formula as the grid size becomes finer. We have also found, in accord with the theory, the 3D solution is independent of the radius of the channel chosen for the calculations. We have used $R =$ 10 Å, 20 Å, and 30 Å for these calculations and found no difference in the final concentrations.

Next, we note that when the cylinder is very wide, $R \rightarrow \infty$, we recover the problem of ion transport between parallel plates of infinite extent. In this limit, both the NP and Poisson equations become strictly one-dimensional (varying in the z direction only). The concentrations are then given exactly by Eq. 9, with the electric potential determined (self-consistently) from the 1D Poisson equation:

$$d^2\phi(z)/dz^2 = (-4\pi e/\epsilon_a)[c^+(z) - c^-(z)] \quad (10)$$

Note that there is only mobile (no embedded) charge in the system, and the dielectric constant is chosen to be that of water. In Fig. 3 flux vs the transmembrane voltage for cylinders of various widths are shown. These were obtained using the full 3D PNP solver code. [Note that flux calculations depend on the appropriate diffusion constants. Here we consider the case that $D_+ = D_-$, as indicated in the caption to Fig. 3.] Once a self-consistent solution of the PNP equations is achieved, the resultant concentrations of the mobile ion species and the electrical potential yield the particle fluxes $\vec{j}^{\pm}(\vec{R})$ via Eq. 2. Each curve obtained from the 3D code is compared with the curve obtained from 1D PNP theory (Eqs. 9 and 10 above). The 1D calculation yields a constant electrical current density. [Note that the flux of electric charge is given by $e(\vec{j}^+ - \vec{j}^-)$.] It is clear that as the channel becomes wider, the fully 3D cylinder results increasingly resemble the 1D parallel plate limit results.

APPLICATION TO THE GRAMICIDIN A CHANNEL

Gramicidin A (GA) is a small polypeptide from *Bacillus brevis* which is known to form an ion channel in the bacterial cell wall or in artificial lipid membranes (Wallace, 1990; Andersen and Koeppe II, 1992; Venkatchalam and Urri, 1983). The GA channel is a β-helix dimer, comprised of identical subunits A and B (cf. Fig. 4 *a*), which forms a narrow open pore permeable to simple monovalent cations K^+, Na^+, and Cs^+. The 3D structure of the dimer is known from 2D NMR and NOE spectroscopy studies to a resolution of 0.86 Å (Arsen'ev et al., 1986). The GA sequence consists of alternating L and D nonpolar amino acids which permit nonpolar side groups to extend into the membrane while the pore is lined by polar peptide groups (see Fig. 4 *a*). The single-channel current has been studied (Aidley and Stanfield, 1996; Hille, 1992) under a variety of conditions.

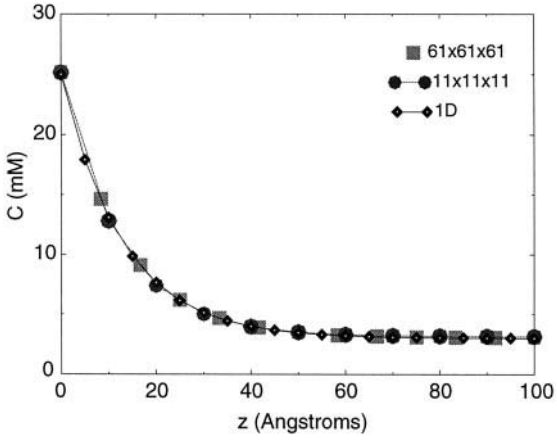

FIGURE 2 Positive ion density for the case of linear electric potential drop of 200 mV across cylinder length $L = 100$ Å. Open circles represent the 1D analytical solution when $c_0 = 25$ mM and $c_L = 3$ mM. Large, filled circles correspond to the 3D solution on a $11 \times 11 \times 11$ grid. Shaded squares correspond to the 3D solution on a $61 \times 61 \times 61$ grid.

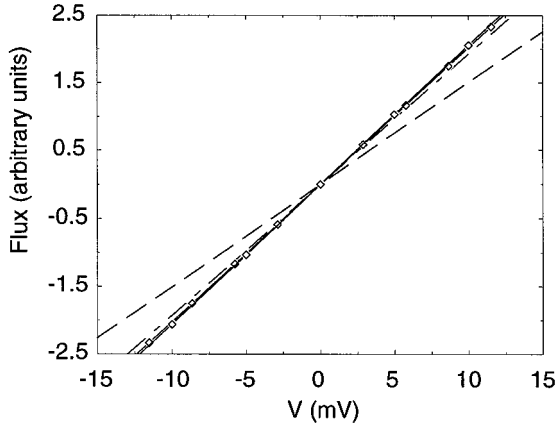

FIGURE 3 Flux versus voltage for three wide cylindrical channels of different width-to-length ratio versus 1D parallel plate PNP solution (*open diamonds*). For the cylinder channels, cylinder dimensions are (radius/length): 5 Å × 100 Å ($R/L = 0.05$), dashed line; 5 Å × 30 Å ($R/L = 0.17$), dot-dashed line; 10 Å × 30 Å ($R/L = 0.33$), open circles. Salt concentrations at the entrance and the exit from the channel are $c_0 = 25$ mM and $c_L = 3$ mM; diffusion constants are $D_+ = D_- = 1.27 \times 10^{-6}$ cm^2/s.

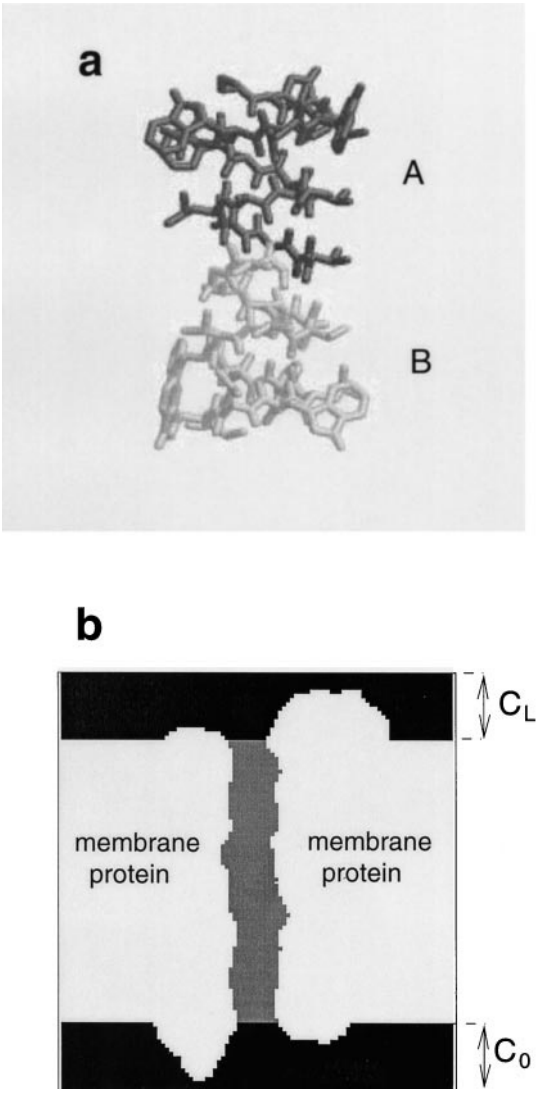

FIGURE 4 (*a*) Gramicidin A dimer. The two subunits are colored in light and dark gray and marked A and B, respectively; (*b*) gramicidin lattice scheme. A 2D cut through the center of the simulation box along the *z* axis illustrates the grid representation of the protein and the membrane. The membrane and the protein region are shown in white, solvent reservoirs are shown in black; the channel region (where mobile ion concentrations are variable) is shown in gray. Grid size is 91 × 91 × 91; the length of the simulation box is 30 Å.

Because it is relatively small and well characterized experimentally, GA has become a focal point for theoretical efforts to explain the mechanism of ionic conduction in protein channels (Barcilon et al., 1992; Roux and Karplus, 1993; Andersen and Feldberg, 1996). In the present work we have utilized PNP theory to calculate this current as a function of voltage applied across the channel.

The system considered consists of a polypeptide dimer, a membrane surrounding it, a pore region inside the gramicidin helix and, finally, inner and outer solvent regions representing the electrolyte inside and outside of the cell membrane. The layout of the GA channel on the grid is shown in Fig. 4 *b*. The coordinates of heavy atoms of the protein (Arsen'ev et al., 1986) were taken from the Protein Data Bank (Bernstein et al., 1977). Partial charges for the GA atoms were taken from the AMBER86 force field (Pearlman et al., 1991). Atomic radii were taken from Delphi (Nicholls et al., 1990); the radii of the polar hydrogens were set to 1.0 Å. The membrane and protein region (white area in Fig. 4 *b*) is described by the low dielectric constant $\epsilon_m = 2$. Salt is excluded from the interior of this region. The high dielectric constant $\epsilon_a = 80$ is assigned to the aqueous region, i.e., the volume outside of the protein-membrane region (black and gray regions of Fig. 4 *b*). As indicated above, the electric potential is set to assigned values (reflecting the applied voltage) along the bottom and top faces of the simulation box. On the side faces it is set by interpolating linearly between top and bottom potential values. In the regions indicated in black, mobile ion concentrations are held to fixed "bath values," whereas in the gray region mobile ion concentrations are variable and are determined by solving the PNP equations self-consistently.

It should be noted that our choice of dielectric response distribution may be oversimplified. The dielectric constant assigned to water in highly restrictive environments where full molecular rotation is inhibited is considerably lower than 80 (Bokris and Khan, 1993). At the same time the appropriate epsilon for the protein environment may be somewhat higher than the traditionally chosen value 2, which accounts only for electronic polarizability of the molecule. It was indicated recently (Warshel and Russell, 1984; Sharp and Honig, 1990) that vibrational polarizability and conformational relaxation can be essential in the dielectric response of the protein, and it is possible to account for these contributions by setting the dielectric constant to a higher value, such as 5. Taking $\epsilon_a = 80$ in the present study reflects the fact that the loss of dielectric screening by water in the channel is probably compensated, to some extent, by the response of the channel itself to the presence of ions. Furthermore, the value $\epsilon_m = 2$ was chosen for the protein and membrane region for the calculations reported in this work after considering the fact that the α-helix comprising the pore lining is a rigid structure, i.e., that vibrations of polar groups in the backbone itself are restricted by mutual interactions. To elucidate the effect of a lower dielectric constant ratio ϵ_a/ϵ_m on the current-voltage characteristics produced by the PNP calculations, we performed additional calculations with $\epsilon_a = 30$ and $\epsilon_m = 5$. The resulting current-voltage curve coincides with the one produced when ϵ_a and ϵ_m are set to 80 and 2, respectively, if one sets the diffusion constant a factor of 1.37 times higher than the diffusion constant chosen for the $\epsilon_a = 80$, $\epsilon_m = 2$ case. (See the discussion of the choice of diffusion constants below.) Also, we note that the computation time increased substantially when the lower dielectric constant for the water was chosen [taking several hours/point on our workstation (see Computational Methods)]. This increase can be traced to the strong electric fields generated by the point charges embedded in the gramicidin molecule, which are less shielded in a low dielectric medium.

Within the PNP theory the computed steady-state ionic currents scale linearly with the corresponding diffusion constants. The diffusion constants for the positive and negative ions, e.g., K^+ and Cl^-, have been measured to be approximately equal to each other in bulk electrolyte ($D_+ = D_- = 10^{-5}$ cm^2/s) (Hille, 1992). There is no experimental measurement of appropriate values for these constants inside the channel. A molecular dynamics simulation of an ion inside a water-filled cylindrical pore having approximately the same dimensions as the GA ion channel yielded diffusion constants two to three times smaller (depending on ion species) than their bulk values (Lynden-Bell and Rasaiah, 1996). In our calculations we have found that the values $D_+ = D_- = 1.27 \times 10^{-6}$ cm^2/s gave results consistent with experimental observations, and these values were used for all our calculations (with $\epsilon_a = 80$, $\epsilon_m = 2$). No further adjustment of parameters was attempted.

To understand the effect of partial charges in the GA protein on the transport of mobile ions through the channel, an additional calculation was performed with no partial charges on the GA atoms (uncharged GA). For both calculations the ionic strengths of salt in the external regions were set to 500 mM at the channel entrance and 40 mM at its exit. The current-voltage relations for GA and uncharged GA are shown in Fig. 5. The large difference in current calculated for GA and uncharged GA demonstrates that the embedded charge distribution in the channel molecule significantly influences current through the channel.

For the GA protein with no partial charges on its atoms and $D_+ = D_-$, the net PNP current is essentially antisymmetric with respect to the direction of the applied voltage. This situation is illustrated in Fig. 6, where the positive and the negative ion currents are shown separately. Figure 9 shows the potential and the positive ion density along the channel center axis, $r = 0$, as discussed in detail below.

In Fig. 7 the electrostatic potential distribution around the channel is shown for both GA and uncharged GA. The corresponding positive ion charge density profiles are shown in Fig. 8.

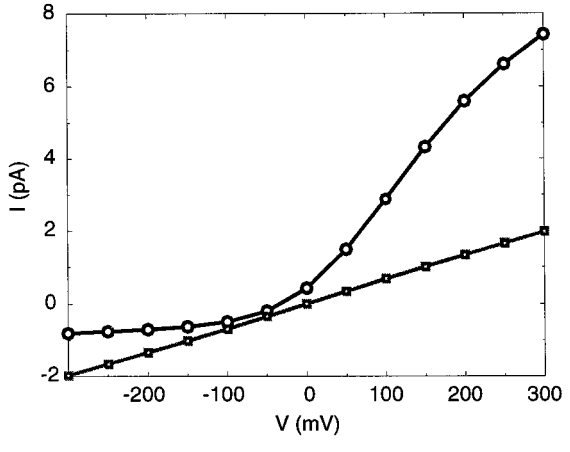

FIGURE 5 Current-voltage characteristics for charged GA (*circles*) and uncharged GA (*squares*). Ionic strengths in the lower and upper reservoirs are $c_0 = 500$ mM and $c_L = 40$ mM, respectively. Diffusion constants are $D_+ = D_- = 1.27 \times 10^{-6}$ cm^2/s.

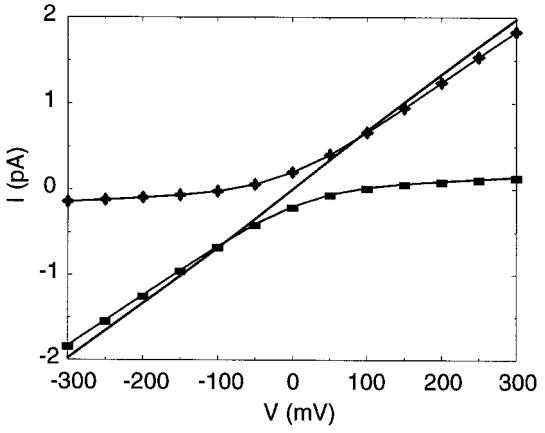

FIGURE 6 Current-voltage characteristics for the uncharged GA. Solid line is the total current, the line with "+" represents positive ion current, line with "−", represents negative ion current.

For the uncharged GA, the change in the potential along the channel is smooth (Fig. 7 *a*). It is especially clear from Fig. 9 *a* that the shape of the potential in this case is largely due to the external linear potential drop across the membrane. For this parameter set, the potential generated by the mobile charge density has a small effect on the current through the channel. In contrast, for the GA with partial charges turned on, one observes a nonuniform electric potential distribution inside and around the channel (see Fig. 7 *b*) and, in particular, a large potential "well" roughly in the center of the channel. In Fig. 8 *b*, in which the corresponding positive mobile charge density is shown, a significant peak in the density is observed in the center of the channel. Comparison of the electric potential and density profiles along the center of the channel in Fig. 9, *a* and *b* for charged and uncharged GA demonstrates the significant modifications induced by the partial charges on the atoms which are exposed into the channel. The GA with partial charges is permeable mainly to positive ions; the local positive ion density rises as high as 8 M. In contrast, the concentration of the negative ions in the channel is very low for all voltages (see Fig. 9 *b*). Additionally, in Fig. 9 *a* the electrostatic potential is shown for two external voltages, applied in opposite directions. Both profiles feature a potential well inside the channel which attracts the mobile positive charges into the channel while preventing the negative charges from flowing inside at all voltages.

Consequences of this charge selectivity of the GA molecule for the electric current through the GA channel are shown in Fig. 10, where the total current as well as the currents of the positive and the negative ions are plotted separately. In this case (in contrast to what is observed in the simple cylinder or uncharged GA case), the negative ion current is essentially negligible. Because of the concentration gradient this current exhibits no symmetry with respect to direction of the applied voltage. The rectification of the

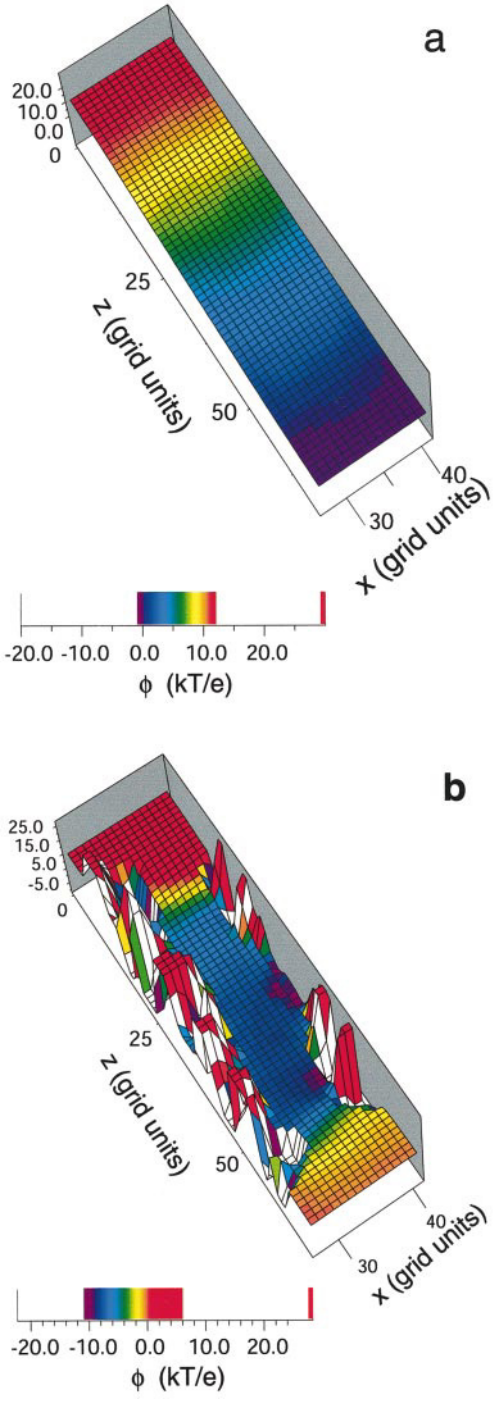

FIGURE 7 Electrostatic potential around the GA channel calculated via PNP theory. Potential variation over a vertical plane slicing through the center of the computational box is depicted, when (*a*) there are no charges on atoms (uncharged GA); (*b*) partial charges are set on the GA atoms according to AMBER86 force field. Ionic strengths in the lower and upper reservoirs are c_0 = 500 mM and c_L = 40 mM, respectively. Potential difference across the membrane is 300 mV. [Note the difference in color scales for panels (*a*) and (*b*).

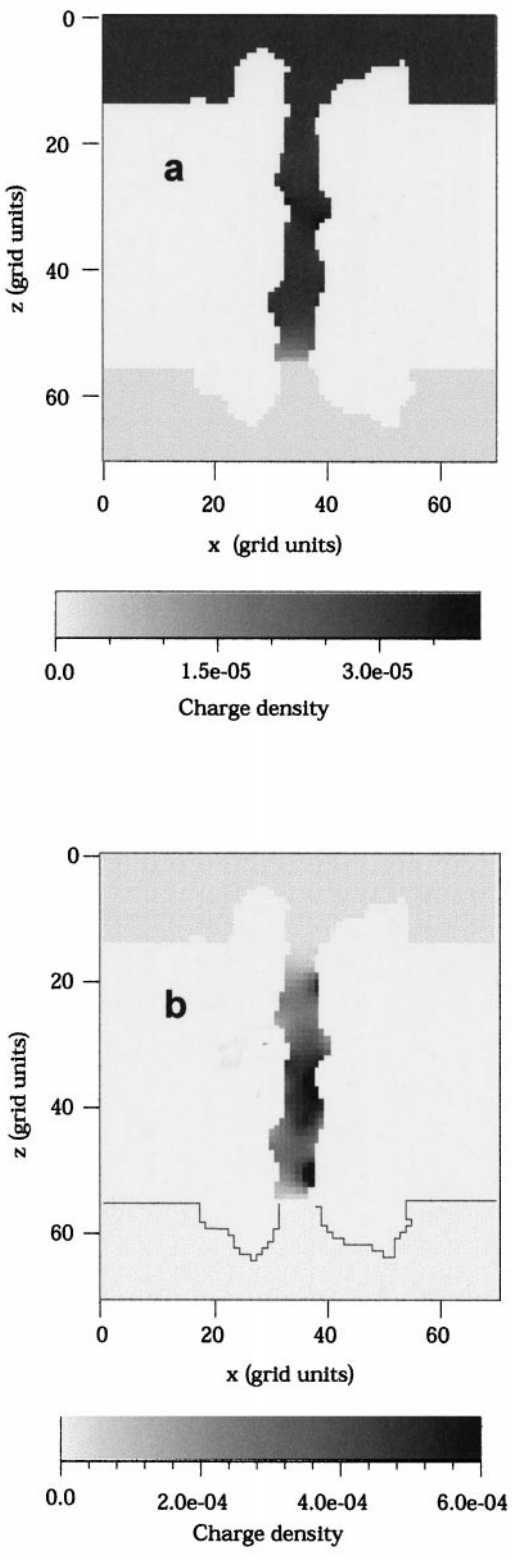

FIGURE 8 Positive ion density distribution inside the GA channel along plane described in Fig. 7, when (*a*) there are no charges on atoms (uncharged GA); (*b*) partial charges are set on the GA atoms according to AMBER86 force field. Ionic strengths in the lower and upper reservoirs are c_0 = 500 mM and c_L = 40 mM, respectively. Potential difference across the membrane is 300 mV. [Note the difference in shading scales for panels (*a*) and (*b*).]

current when the ionic strength on one side of the membrane is different from the ionic strength on the other side is observed only for the charged GA, as is the saturation of the current at moderate voltage differences (discussed below).

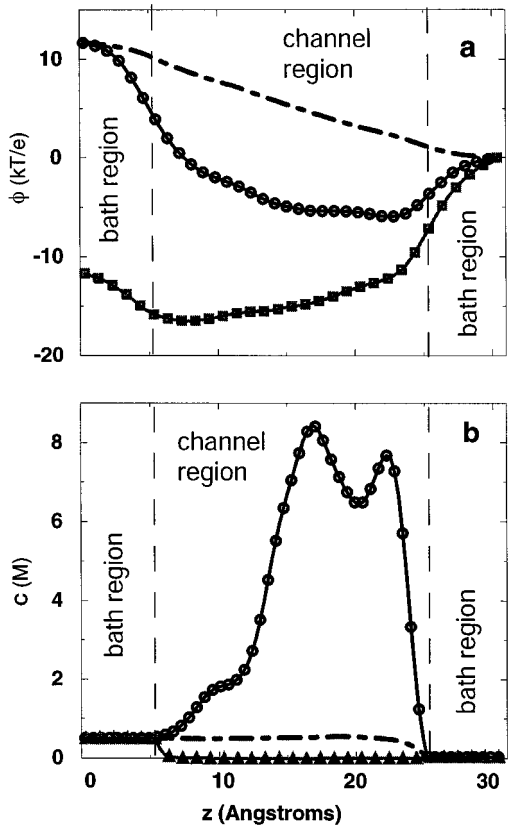

FIGURE 9 (*a*) Electrostatic potential at the center ($r = 0$) of the GA channel plotted along z (channel)-axis obtained from the PNP calculation. The dot-dashed line represents $\phi(r = 0, z)$ for the channel with no fixed partial charges; line with circles is the corresponding result for the channel with partial charges turned on. In both cases the external potential across the membrane is set to +300 mV. The line with squares shows $\phi(r = 0, z)$ for the channel with partial charges on and external potential across the membrane is set to −300 mV. Ionic strengths in the entrance and exit reservoirs are $c_0 = 500$ mM and $c_L = 40$ mM. (*b*) Ionic concentration at the center ($r = 0$) of the GA channel plotted along z (channel)-axis obtained from the PNP calculation. Dot-dashed line represents $c^+(r = 0, z)$ for the channel with no fixed partial charges; the line with circles is the same function in the channel with partial charges turned on. The line with triangles represents the density of negative ions $c^-(r = 0, z)$ in the channel with partial charges on. Ionic strengths in the lower and upper reservoirs are $c_0 = 500$ mM and $c_L = 40$ mM; the external potential across the membrane is set to +300 mV.

A closer look inside the channel at the mobile charge and potential distributions enables one to understand how the channel protein molecule influences the charge density flowing into it. A more detailed consideration of the density profile dependence on the external potential difference across the membrane and the external salt concentrations allows us to identify possible attractive sites for the positive ions. Before presenting this analysis we address the important question of how well PNP model results compare with known experimental properties of GA channels.

For comparison with experiment we have chosen results of single-channel recording of GA in CsCl salt reported by the group of O. Andersen (Oiki et al., 1994; Mazet et al., 1984). In these measurements and in our corresponding

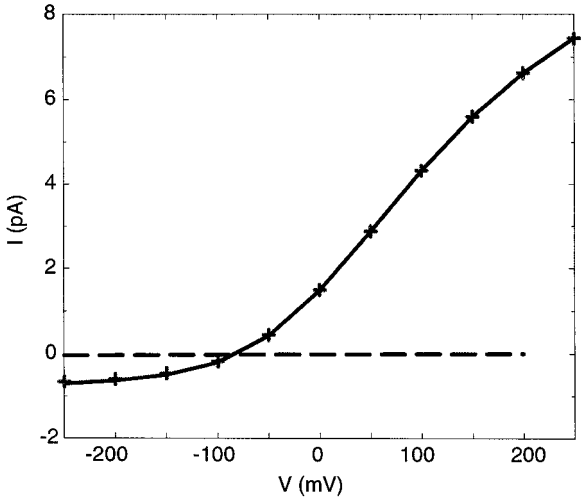

FIGURE 10 Current-voltage characteristics for the GA with partial charges on the atoms. Solid line is the total current, the line with "+" represents positive ion current (indistinguishable from positive ion current). Line with "−" represents negative ion current. Ionic strengths in the lower and upper reservoirs are $c_0 = 500$ mM and $c_L = 40$ mM, respectively.

calculations the salt concentrations on the channel boundaries were taken to be equal. Current-voltage relations were generated for two different salt concentrations: 0.01 M and 1.0 M. In Fig. 11, current calculated for 1 M ionic concentrations on both sides of the membrane is plotted versus potential difference across the membrane and compared to experimental data of Oiki et al. (1994). The calculated curve closely resembles the experimental one. Both experimental and calculated curves indicate that the GA channel exhibits no rectification and there is essentially no saturation of the current even at high voltages. The *I-V* behavior at low salt concentrations is significantly different. In Fig. 12 the calculated $I - V$ curve is plotted for the external salt concen-

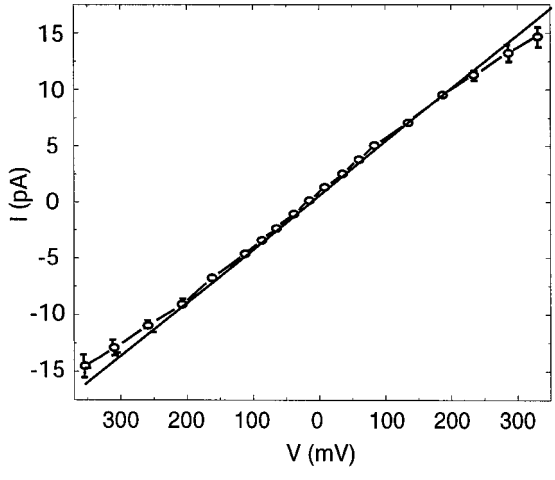

FIGURE 11 Current versus voltage calculated via PNP for the GA channel (*solid line*). Ionic concentrations on both sides of the membrane are 1 M. Circles represents the experimental data taken from Oiki et al. (1994).

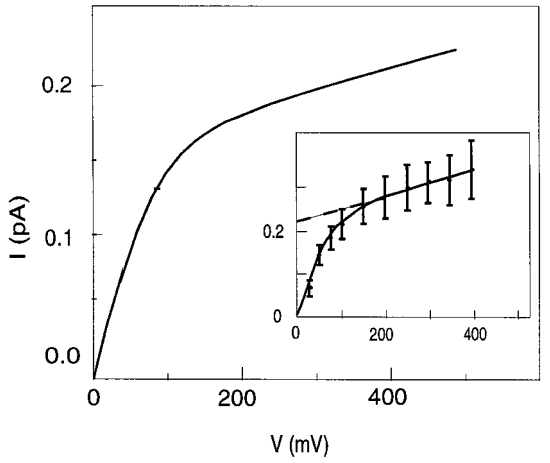

FIGURE 12 Current versus voltage calculated via PNP for the GA channel. Ionic concentrations on both sides of the membrane are 0.01 M. Shown in the inset are the experimental data taken from Andersen (1983).

tration of 0.01 M and compared to the experimental curve (see inset) from Andersen (1983). For this concentration the model again works reasonably well. At negative voltages (not shown) the line extends antisymmetrically; thus there is no rectification. The model also reproduces the saturation of the current at high voltage, which is an important property of many biological channels and is not reproduced by the PNP model under consideration here if partial charges on the channel atoms are not taken into account.

Let us now study the charge density profile inside the channel as the current flows through it. At moderate to high external salt concentrations (Fig. 13 *a* and *b*) the calculated density profile features four symmetrically located density maxima; the height of these peaks rapidly increases as the concentration rises from moderate (~1 M) to high (~10 M) (Fig. 13 *b*). At very high concentrations the concentration profile does not depend sensitively on external salt concentrations or the external potential (Fig. 13 *a*). From this figure it is clear that at a variety of salt concentrations the locations of the peaks observed are independent of external conditions. These peaks can be identified as sites of attraction (or residence) for positive ions traveling through the channel. In Fig. 14 their location is schematically represented with large spheres placed inside the GA dimer channel according to the locations of the ionic density maxima found in PNP calculations, and corresponding to the four peaks of the density observed in Fig. 13. The atomic groups closest to this density maxima are polar oxygens of the peptide backbone in the following amino acids (along the channel):

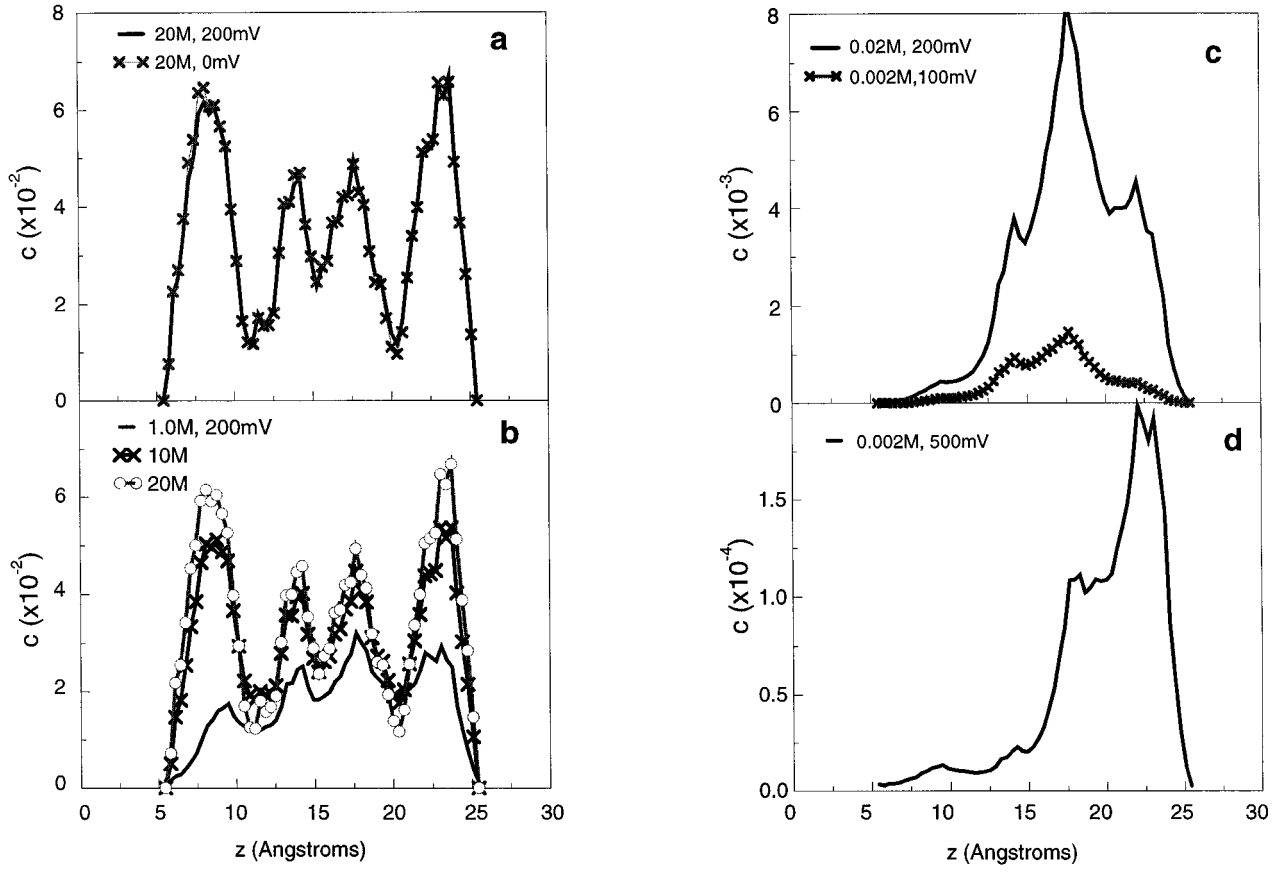

FIGURE 13 Mobile ion charge distribution along the *z*-(channel) axis. $c_0 = c_L$ for all lines. The appropriate applied potential difference and entrance/exit concentrations are indicated on each panel. [Note that the applied voltage is 200 mV for all curves in panel (*b*).]

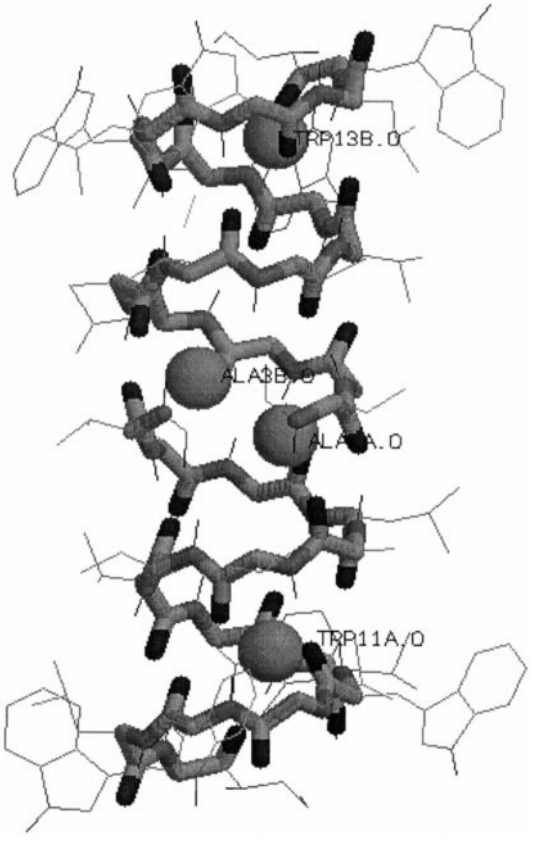

FIGURE 14 Schematic picture of the GA dimer. Centers of the spheres represent the calculated positive charge maximum positions inside the channel. Size of these spheres is chosen arbitrarily.

Trp-11 and Ala-3 in subunit A, Ala-3 and Trp-13 in subunit B.

At low salt concentrations and moderate voltages only one or two charge density maxima occur roughly in the center of the channel, as shown, for example, in Fig. 13 *c* for the external salt concentration 0.02 M and a 200 mV potential difference across the membrane. The occurrence of these central attractive sites is nearly independent of external conditions, while the attractive sites at the entrance/exit of the channel are not pronounced in this regime. The persistence of the central attractive sites revealed in our calculations suggests that the ionic permeability through the GA channel is influenced by the molecular structure of the protein in the middle of the channel. The experimentally observed variation of the ionic current upon the substitution of certain amino acids in the middle of the channel (e.g., Ala-1 to Tyr), and the relative lack of variation of the ionic current when Trp-13 is replaced by Val or Tyr (Mazet et al., 1984) support this hypothesis. A very high voltage drop across the membrane (500 mV) at low salt concentrations shifts the residence site to the side (exit) of the channel (Trp-13) (see Fig. 13 *d*) where the potential created by this attracted positive charge compensates the external potential and prevents more positive charge from going into the channel.

An estimation of the location of cation binding sites from the experimental structural data was previously provided by Urri et al. (1982a, b) and later by Jing et al. (1995) using NMR spectroscopy with ^{13}C-labeled gramicidin incorporated into lipid micelles. Changes in the NMR spectrum due to the presence of the Na^+ cation were observed for the carbonyl carbon of Trp-11 and Trp-13, which is in accord with our results. Studies performed using solid-state NMR indicated that the carbonyls of Leu-10, Leu-12, and Leu-14 were affected by the presence of Na^+ (Smith et al., 1995; Separovic et al., 1994). Thus, most of the available structural experimental data indicate that there is a cation binding site near the entrance of the channel at a distance of 9–10 Å from the center of the dimer. A recent study of the binding site of sodium in the GA channel (Woolf and Roux, 1997) combined available experimental data with molecular dynamics simulation in order to refine the cation position at the binding site in the channel. This study indicated that the cation is located off the center of the channel and is coordinated by carbonyl oxygens of Val-8, Leu-10, Trp-15, and two single file water molecules. No large distortions of the channel structure due to the presence of the ion in the channel were observed and the largest deviation from its equilibrium position in the ion-free channel was exhibited by the carbonyl group of Leu-10–Trp-11 amide plane. This is also in accord with our result of finding large density peaks near Trp-11 and Trp-13. It appears that most previous authors find no evidence that there is a cation binding site in the center of the channel (Urri et al., 1982b; Separovic et al., 1994; Woolf and Roux, 1997), while our calculations indicate the existence of the deep potential well and therefore a large density peak near Ala-3. We believe that further investigations are needed to clarify this discrepancy between our results and the experimental studies. One possible explanation may be that the channel is more rigid in the center than in the entrance regions; therefore, its structure does not change significantly when the ion binds at the center of the dimer and hence cannot be resolved with NMR spectroscopy. Another explanation may be that water molecules, which our model does not explicitly include, are preferentially attracted to this site, thus preventing it from attracting a cation.

DISCUSSION AND CONCLUSIONS

In this paper we have developed a numerical method for solving the 3D Poisson-Nernst-Planck (PNP) equations. The method is comprised of self-consistent solution of elliptic partial differential equations using straightforward successive over-relaxation (SOR) techniques. Although this solution procedure can be applied to a variety of problems in electrochemistry, we have focused here on an important biophysical process, namely transport of simple ions through channel proteins embedded in biological cell walls. We considered in detail the case of the nearly cylindrical pore created by the GA dimer, a system that has been much

studied experimentally and theoretically. The flexibility of our method allowed us to treat the full 3D structure of the gramicidin protein, and all partial charges embedded in it. We computed the induced ion current associated with a range of applied voltages, i.e., the current voltage characteristic, which agreed well with recent experimental measurements of Andersen et al.

Obviously, the model and theory presented in this paper are greatly oversimplified, and despite their apparent success we should keep in mind their shortcomings. The following issues are particularly important:

1. The PNP model presented here is based on a continuum picture. Ion sizes as well as the molecular nature of water are disregarded;
2. The PNP theory is a mean field approximation in which important correlations are neglected. Despite its known successes, its validity in the narrow channel environment (where the average number of ions at any time is typically one or less) should be questioned. Ion-ion correlations such as the possible exclusion of an ion from a channel that contains another ion of the same charge sign are not included in this theory;
3. Some parameters and details of the calculation are uncertain due to lack of knowledge about the actual system, even though they could, in principle, be included within the framework of the present treatment. For example, as discussed above, the dielectric properties of water in the channel are not known and the choice of diffusion constant values made for both K^+ and Cl^- in the GA calculation should be regarded as a fitting procedure.

In view of the discussion above, the success of the present calculation is remarkable. We leave for future studies the question how much of this success is due to cancellation of errors between contributing factors and how much because the corrections involved are small. Some improvement of the model may be obtained by considering ion-ion correlations within the mean field level (Coalson et al., 1995). More answers to these issues can, in principle, be provided by MD simulations. However, realistic simulations of this type on relevant length and time scales are beyond our present capabilities. Dynamic Monte Carlo simulations can also shed light on some of the issues by going beyond the mean field level of the theory. Such simulations are currently underway.

APPENDIX 1

Mapping the Nernst-Planck equation to a Laplace equation

Equation 3 can be transformed into the standard 3D Laplace equation with a particular spatially dependent dielectric profile. As noted in the text, a number of efficient grid methods have been developed to solve the 3D Laplace equation (Press et al., 1992; Coalson and Beck, 1998).

Specifically, if we let $c(\vec{R}) = \exp[-\beta V(\vec{R})]\ \psi(\vec{R})$, then Eq. 3 above is equivalent to

$$0 = \vec{\nabla} \cdot (\epsilon_{\text{eff}}(\vec{R})\vec{\nabla}\psi(\vec{R})) \tag{11}$$

with the effective "dielectric profile" $\epsilon_{\text{eff}}(\vec{R}) \equiv \exp[-\beta V(\vec{R})]$. [This effective dielectric constant profile is a mathematical construction that arises in the mapping of a drift-diffusion equation to a Laplace-type equation. It should not be confused with the physical dielectric constant profile which enters into the solution of Poisson's equation for the electric potential distribution; see Eq. 6.] Given its value on the boundary surface, $\psi(\vec{R})$ can now be evaluated by standard lattice relaxation techniques.

Note that if the concentration of Brownian particles on the boundary is Boltzmann-distributed, then $\psi = \psi_0$ (a constant) on the boundaries. The interior solution in this case is also $\psi = \psi_0$, i.e., Boltzmann equilibrium on the boundary implies Boltzmann equilibrium in the interior, and $\vec{j} = 0$. Otherwise, the interior solution is nontrivial and the corresponding flux is nonzero.

APPENDIX 2

Implementation of the successive over-relaxation method for the Nernst-Planck equation

The Nernst-Planck (NP) equation for the mobile ion concentration of a given species is solved by cycling around the lattice and updating each lattice point based on the present value of its nearest neighbors. For notational and diagrammatic simplicity, we will develop the desired formulas for a 2D system. Results for the 3D case follow analogously and are summarized below.

Fig. 15 *a* shows the typical situation in the interior of the flow region in 2D. Each flux vector can be associated with the midpoint of the central grid point and the nearest neighbor it connects to. For example, the flux in the x direction halfway between (i, j) and $(i + 1, j)$ has the lattice (finite difference) representation (cf. Eq. 2):

$$j^{\text{x}}_{\text{i+1}} = c_{\text{i+1,j}} - c_{\text{i,j}} + \beta(V_{\text{i+1,j}} - V_{\text{i,j}})(c_{\text{i+1,j}} + c_{\text{i,j}})/2 \tag{12}$$

[Note that the physical flux is $-Dj^{\text{x}}_{\text{i+1}}/a$, where D is the diffusion constant, a is the lattice spacing, and $j^{\text{x}}_{\text{i+1}}$ is the expression in Eq. 12. However, the factor $-D/a$ cancels out of the following manipulations and is therefore ignored.] The condition that $c_{\text{i,j}}$ is at steady state is that there is no net flux into the point (i, j), i.e.,

$$j^{\text{x}}_{\text{i+1}} - j^{\text{x}}_{\text{i-1}} + j^{\text{y}}_{\text{j+1}} - j^{\text{y}}_{\text{j-1}} = 0 \tag{13}$$

This is simply the lattice version of the NP equation (Eq. 5).

Substituting the explicit expressions for the flux components and solving the resulting equation for the concentration at the central point, one finds:

$$\begin{aligned} c_{\text{i,j}} = \{&c_{\text{i+1,j}} + c_{\text{i-1,j}} + c_{\text{i,j+1}} + c_{\text{i,j-1}} \\ &+ (\beta/2)[(V_{\text{i+1,j}} - V_{\text{i,j}})c_{\text{i+1,j}} - (V_{\text{i,j}} - V_{\text{i-1,j}})c_{\text{i-1,j}} \\ &+ (V_{\text{i,j+1}} - V_{\text{i,j}})c_{\text{i,j+1}} - (V_{\text{i,j}} - V_{\text{i,j-1}})c_{\text{i,j-1}}]\} \\ &\div \{4 - (\beta/2)[(V_{\text{i+1,j}} - V_{\text{i,j}}) - (V_{\text{i,j}} - V_{\text{i-1,j}}) \\ &+ (V_{\text{i,j+1}} - V_{\text{i,j}}) - (V_{\text{i,j}} - V_{\text{i,j-1}})\} \end{aligned}$$

This expression can be written in a more compact form if we label the central point by subscript 0 and all neighboring points by the subscript $i = 1, \ldots, 4$; then:

$$c_0 = \frac{\sum_{\text{i}=1}^{4}[1 + (\beta/2)(V_{\text{i}} - V_0)]c_{\text{i}}}{4 - (\beta/2)\sum_{\text{i}=1}^{4}(V_{\text{i}} - V_0)}, \tag{14}$$

(The ordering of the four nearest neighbor sites is clearly irrelevant.) Then, in an SOR scheme, the point $c_{\text{i,j}}$ is updated according to

$$c_{\text{i,j}} = (1 - w)c^{\text{old}}_{\text{i,j}} + wc_0, \tag{15}$$

where $c^{\text{old}}_{\text{i,j}}$ is the pre-update value of $c_{\text{i,j}}$ and w is a positive weight factor, adjusted to get the most rapid convergence without losing stability.

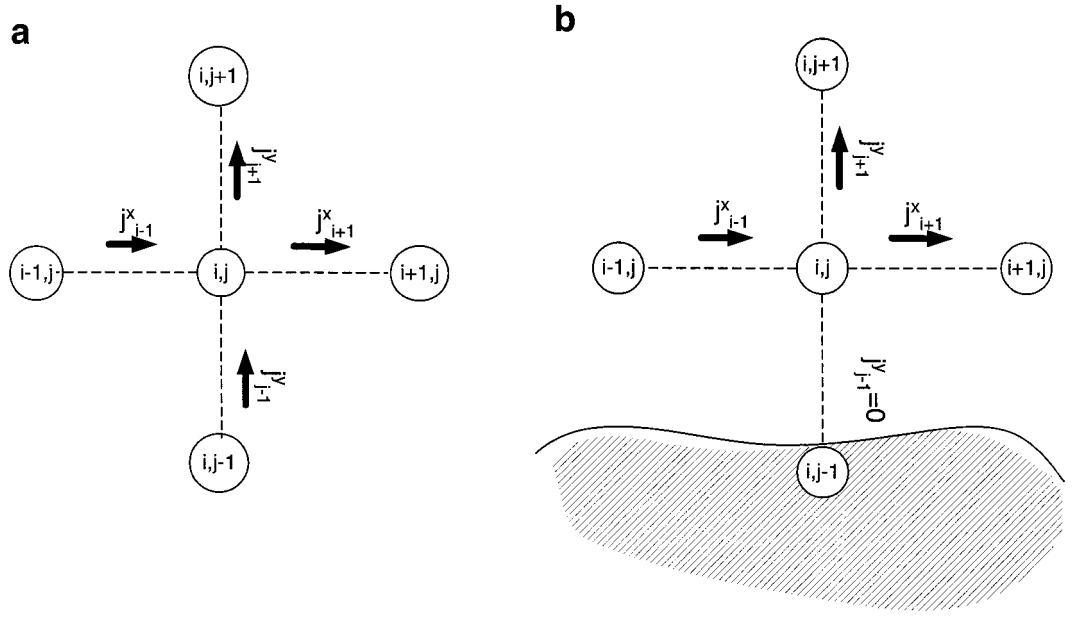

FIGURE 15 Schematic representation of flux into central grid point (i, j) for 2D system: (*a*) central point is surrounded by nearest neighbors which are all in the interior (flow) region; (*b*) one nearest neighbor of the central grid point is external to the (impenetrable) boundary.

In the case that the central point (i, j) is adjacent to an impenetrable boundary surface, as indicated in Fig. 15 *b*, no particles flow through the boundary surface so that, e.g., $j^y_{j-1} = 0$. In this case the condition of steady-state concentration $c_{i,j}$ is

$$j^x_{i+1} - j^x_{i-1} + j^y_{j+1} = 0. \tag{16}$$

Now the concentration of the central point is given in terms of the concentrations of its nearest neighbors, which are interior to the boundary, by:

$$\begin{aligned} c_{i,j} = \{&c_{i+1,j} + c_{i,j+1} + c_{i,j-1} \\ &+ (\beta/2)[(V_{i+1,j} - V_{i,j})c_{i+1,j} + (V_{i,j+1} - V_{i,j})c_{i,j+1} \\ &- (V_{i,j} - V_{i,j-1})c_{i,j-1}]\} \\ &\div \{3 - (\beta/2)[(V_{i+1,j} - V_{i,j}) + (V_{i,j+1} - V_{i,j}) \\ &- (V_{i,j} - V_{i,j-1})]\} \end{aligned}$$

Again, this can be written more compactly using the notation adopted in Eq. 14 above, as:

$$c_0 = \frac{\sum_{i=1}^{3}[1 + (\beta/2)(V_i - V_0)]c_i}{3 - (\beta/2)\sum_{i=1}^{3}(V_i - V_0)}, \tag{17}$$

where the sum runs over points which are nearest neighbors of (i, j) and are in the interior of the flow region (these can be indexed in any order). An analogous procedure applies when more than one nearest neighbor is exterior to the flow region.

In 3D the analysis proceeds in the same way. For a point whose nearest neighbors are all in the interior of the flow region

$$c_0 = \frac{\sum_{i=1}^{6}[1 + (\beta/2)(V_i - V_0)]c_i}{6 - (\beta/2)\sum_{i=1}^{6}(V_i - V_0)}, \tag{18}$$

the sum running over the six nearest neighbors of the central point. If a point lies next to a boundary surface such that one of its nearest neighbors is on the exterior side of the boundary, then

$$c_0 = \frac{\sum_{i=1}^{5}[1 + (\beta/2)(V_i - V_0)]c_i}{5 - (\beta/2)\sum_{i=1}^{5}(V_i - V_0)}, \tag{19}$$

with the sum running over the five nearest neighbors in the interior of the flow region. Analogous formulas follow for the case of two or more nearest neighbors outside the boundary.

We note in passing that the above reasoning applies equally well to the case of constant concentration boundary conditions. Then, in 3D, Eq. 18 is used to update all interior points. Those points which abut the boundary require knowledge of the concentrations of lattice points on the boundary, but the latter are prescribed by the boundary conditions.

The authors thank Professors J. Shin, C. Wilcox, and N. Ben-Tal for helpful discussions, and Professor R. S. Eisenberg for critical comments on the manuscript. A. N. also thanks Professor R. S. Eisenberg for introducing him to the subject of ionic channels and for many illuminating discussions, and professors M. Ratner and Z. Schuss for many helpful discussions.

This work was supported in part by NSF Grant CHE-9633561 (to R. D. C.), a Mellon predoctoral fellowship from the University of Pittsburgh (to M. G. K.), and the NSF of Israel and the German-Israeli DIP (A. N.).

REFERENCES

Aidley, D. J., and P. R. Stanfield. 1996. Ion Channels: Molecules in Action. Cambridge University Press, Cambridge; New York.

Andersen, O. S. 1983. Ion movement through gramicidin a channels. Interfacial polarization effects on single-channel current measurements. *Biophys. J.* 41:135–146.

Andersen, O. S., and S. W. Feldberg. 1996. The heterogeneous collision velocity for hydrated ions in aqueous solution is 10^4 cm/s. *J. Phys. Chem.* 100:4622–4629.

Andersen, O. S., and R. E. Koeppe II. 1992. Molecular determinants of channel function. *Physiol. Rev.* 72:S89–S158.

Arsen'ev, A. S., A. L. Lomize, I. L. Barsukov, and V. F. Bystrov. 1986. Gramicidin A transmembrane ion-channel. Three-dimensional structure reconstruction based on NMR spectroscopy and energy refinement. *Biol. Membr.* 3:1077–1104.

Barcilon, V., D. P. Chen, and R. S. Eisenberg. 1992. Ion flow through narrow membrane channels. II. *SIAM J. Appl. Math.* 52:1405–1425.

Ben-Tal, N., and R. D. Coalson. 1994. Dielectric constant effects on the energetics of oppositely charged colloids: a lattice field theory study. *J. Chem. Phys.* 101:5148–5166.

Bernstein, F. C., T. F. Koetzle, G. J. B. Williams, E. F. Meyer, M. D. Brice, J. R. Rodgers, O. Kennard, T. Shimanouchi, and M. Tasumi. 1977. The protein data bank: a computer-based archival file for macromolecular structures. *J. Mol. Biol.* 112:535–542.

Bokris, J. O. and S. U. M. Khan. 1993. *In* Surface Electrochemistry. Plenum Press, New York.

Chandrasekhar, S. 1943. Stochastic problems in physics and astronomy. *Rev. Mod. Phys.* 15:1–89.

Chen, D. P., V. Barcilon, and R. S. Eisenberg. 1992. Constant fields and constant gradients in open ionic channels. *Biophys. J.* 61:1372–1393.

Chen, D. P., and R. S. Eisenberg. 1993a. Charges, currents, and potentials in ionic channels of one conformation. *Biophys. J.* 64:1405–1421.

Chen, D. P., and R. S. Eisenberg. 1993b. Flux, coupling, and selectivity in ionic channels of one conformation. *Biophys. J.* 65:727–746.

Chen, D. P., J. Lear, and R. S. Eisenberg. 1997a. Permeation through an open channel: Poisson-Nernst-Planck theory of a synthetic channel. *Biophys. J.* 72:97–116.

Chen, D. P., L. Xu, A. Tripathy, G. Meissner, and R. S. Eisenberg. 1997b. Permeation through the calcium release channel of cardiac muscle. *Biophys. J.* 73:1337–1354.

Chernyak, Y. B. 1995. A universal steady-state I-V relationship for membrane current. *IEEE Trans.* 42:1145–1157.

Coalson, R. D., and T. L. Beck. 1998. Poisson-Boltzmann type equations: numerical methods. *In* Encyclopedia of Computational Chemistry, P. von Rague Schleyer, editor. J. Wiley & Sons, New York. 2086–2100.

Coalson, R. D., and A. D. Duncan. 1992. Systematic ionic screening theory of macroions. *J. Chem. Phys.* 97:5653–5661.

Coalson, R. D., A. M. Walsh, A. Duncan, and N. Ben-Tal. 1995. Statistical mechanics of a coulomb gas with finite size particles: a lattice field theory approach. *J. Chem. Phys.* 102:4584–4594.

Connolly, M. L. 1983. Solvent-accessible surfaces of proteins and nucleic acids. *Science.* 221:709–713.

Cooper, K., E. Jakobsson, and P. Wolynes. 1985. The theory of ion transport through membrane channels. *Prog. Biophys. Molec. Biol.* 46: 51–96.

Cowan, S. W., T. Schrimer, G. Rummel, M. Steiert, R. Ghosh, R. A. Pauptit, J. N. Jansonius, and J. P. Rosenbush. 1992. Crystal structures explain properties of two *E. coli* porins. *Nature.* 358:727–733.

Doyle, D. A., J. M. Cabral, R. A. Pfuetzner, A. Kuo, J. M. Gulbis, S. L. Cohen, B. T. Chait, and R. MacKinnon. 1998. The structure of the potassium channel: molecular basis of K^+ conduction and selectivity. *Science.* 280:69–77.

Eisenberg, R. S. 1996. Computing the field in proteins and membranes. *J. Membr. Biol.* 150:1–25.

Eisenberg, R. S. 1998. Ionic channels in biological membranes: natural nanotubes. *Acc. Chem. Res.* 31:117–123.

Elber, R., D. P. Chen, D. Rojewska, and R. S. Eisenberg. 1995. Sodium in gramicidin: an example of permion. *Biophys. J.* 68:906–924.

Fishman, H. M. 1985. Relaxation, fluctuations and ion transfer across membranes. *Prog. Biophys. Mol. Biol.* 46:127–162.

Hille, B. 1992. Ionic Channels of Excitable Membranes. Sinauer Associates Inc., Sunderland, MA.

Jing, N., K. U. Prasad, and D. W. Urri. 1995. The determination of binding constants of micellar-packed gramicidin a by ^{13}C- and ^{23}Na-NMR. *Biophys. Biochim. Acta.* 1238:1–11.

Kreusch, A., and G. E. Schulz. 1992. Refined structure of the porin from *Rhodobacter blastica. J. Mol. Biol.* 243:891–905.

Levitt, D. G. 1991a. General continuum theory for multiion channel. I. Theory. *Biophys. J.* 59:271–277.

Levitt, D. G. 1991b. General continuum theory for multiion channel. II. Application to acetylcholine channel. *Biophys. J.* 59:278–288.

Luty, B. A., M. E. Davis, and J. A. McCammon. 1992. Solving the finite-difference non-linear Poisson-Boltzmann equation. *J. Comp. Chem.* 13: 1114–1118.

Lynden-Bell, R. M., and J. C. Rasaiah. 1996. Mobility and solvation of ions in channels. *J. Chem. Phys.* 105:9266–9280.

Mazet, J. L., O. S. Andersen, and R. O. Koeppe II. 1984. Single-channel studies on linear gramicidins with altered amino acid sequences. *Biophys. J.* 45:263–276.

Newman, J. S. 1991. Electrochemical Systems. Prentis-Hall Inc., Englewood Cliffs, NJ.

Nicholls, A., K. A. Sharp, and B. Honig. 1990. DelPhi V3.0. Columbia University, New York.

Novak, J. P. 1997. Calcium ion current from an extracellular electrolyte toward a channel opening in an insulating membrane: quantitative model with rotational symmetry. *IEEE Trans.* 44:940–947.

Oiki, S., R. O. Koeppe II, and O. S. Andersen. 1994. Asymmetric gramicidin channels: heterodimeric channels with a single F_6Val^1 residue. *Biophys. J.* 66:1823–1832.

Pearlman, D. A., D. A. Case, J. C. Caldwell, G. L. Seibel, U. C. Singh, P. Weiner, and P. A. Kollman. 1991. AMBER 4.1. University of California, San Francisco.

Press, W. H., B. P. Flannery, S. A. Teukolsky, and W. T. Vetterling. 1992. Numerical Recipes in Fortran: The Art of Scientific Computing. Cambridge University Press, Cambridge, New York.

Ramanan, S. V., V. Mesimeris, and P. R. Brink. 1994. Ion flow in the bath and flux interactions between channels. *Biophys. J.* 66:989–995.

Riveros, O. J., T. L. Croxton, and W. M. Armstrong. 1989. Liquid junction potentials calculated from numerical solutions of the Nernst-Planck and Poisson equations. *J. Theor. Biol.* 140:221–230.

Roux, B., and M. Karplus. 1993. Ion transport in the gramicidin channel: free energy of the solvated ion in a model membrane. *J. Am. Chem. Soc.* 115:3250–3260.

Selberherr, S. 1984. Analysis and Simulation of Semiconductor Devices. Springer-Verlag, Wien.

Separovic, F., J. Gehrmann, T. Milne, B. A. Cornell, S. Y. Lin, and R. Smith. 1994. Sodium ion binding in the gramicidin A channel: solid-state NMR studies of the tryptophan residues. *Biophys. J.* 67:1495–1500.

Sharp, K. A., and B. Honig. 1990. Electrostatic interactions in macromolecules: theory and applications. *Annu. Rev. Biophys. Biophys. Chem.* 19:301–332.

Slotboom, J. W. 1969. Iterative scheme for 1- and 2-dimensional d.c.-transistor simulation. *Electron. Lett.* 5:677–678.

Smith, R., D. E. Thomas, A. R. Atkins, F. Separovic, and B. A. Cornell. 1995. Solid-state ^{13}C-NMR studies of the effects of sodium ions on the gramicidin A ion channel. *Biophys. Biochim. Acta.* 1238:1–11.

Song, L., M. R. Hobauch, C. Shustak, S. Cheley, H. Bayley, and J. E. Gouaux. 1996. Structure of staphylococcal alpha-hemolysin, a heptameric transmembrane pore. *Science.* 274:1859.

Syganow, A., and E. von Kitzing. 1995. Integral weak diffusion and diffusion approximations applied to ion transport through biological ion channels. *J. Phys. Chem.* 99:12030–12040.

Unwin, N. 1995. Acetylcholine receptor channel imaged in the open state. *Nature.* 373:586–596.

Urri, D. W., K. U. Prasad, and T. L. Trapane. 1982a. Location of monovalent cation binding sites in the gramicidin channel. *Proc. Natl. Acad. Sci. USA.* 79:390–394.

Urri, D. W., J. T. Walker, and T. L. Trapane. 1982b. Ion interactions in $(1\text{-}^{13}c)d\text{-}val^8$ and $dleu^14$ analogues of gramicidin a, the helix sense of the channel, and the location of ion binding sites. *J. Membr. Biol.* 69: 225–231.

Venkatchalam, M., and P. Urri. 1983. Theoretical perspectives of ion-channel electrostatics, continuum and microscopic approach. *J. Comput. Chem.* 4:461–469.

Wallace, B. A. 1990. Gramicidin channels and pores. *Annu. Rev. Biophys. Biophys. Chem.* 19:127–157.

Walsh, A. M., and R. D. Coalson. 1994. Lattice field theory for spherical macroions in solution: calculation of equilibrium pair correlation functions. *J. Chem. Phys.* 100:1559–1566.

Warshel, A., and S. T. Russell. 1984. Calculations of electrostatic interactions in biological systems and in solutions. *Q. Rev. Biol.* 17:283–422.

Weiss, M. S., and G. E. Schulz. 1992. Structure of porin refined at 1.8 Å resolution. *J. Mol. Biol.* 227:493–509.

Woolf, T. B., and B. Roux. 1997. The binding site of sodium in the gramicidin A channel: comparison of molecular dynamics with solid-state NMR data. *Biophys. J.* 72:1930–1945.

Woolley, G. A., P. C. Biggin, A. Schultz, L. Lien, D. C. Jaikaran, J. Breed, K. Crowhurst, and M. S. Sansom. 1997. Intrinsic rectification of ion flux in alamethicin channels: studies with an alamethicin dimer. *Biophys. J.* 73:770–778.